



Evaluation of Ultimate Seismic Capacity of Existing Seismically Eccentric RC Buildings by Ambient Vibration Measurement

H. Hinata⁽¹⁾, T. Hida⁽²⁾, T. Takada⁽³⁾

⁽¹⁾ *Researcher, Kajima Corporation, hinatah@kajima.com*

⁽²⁾ *Assistant Professor, the University of Tokyo, hida@load.arch.t.u-tokyo.ac.jp*

⁽³⁾ *Professor, the University of Tokyo, takada@load.arch.t.u-tokyo.ac.jp*

Abstract

Story collapses of many RC buildings due to torsional response which were induced mainly by seismic eccentricity of buildings, were reported in the 1995 Kobe earthquake. Therefore, it is important to grasp the torsional response properties for evaluating ultimate seismic capacity of existing RC building. The modulus of eccentricity has been introduced in the Japanese current seismic design standards, which reflects spatial non-uniformity of mass and horizontal rigidity of seismic resistant elements such as columns and seismic walls. However, the modulus does not directly relate to the torsional response which depends on building vibrational behavior and input motions. Moreover, since the vibration behavior of existing buildings varies in time, in order to capture the vibrational behavior of existing buildings appropriately, the design conditions and original drawings are not sufficient to reflect the actual condition of the buildings which had experienced some damage from past earthquakes.

In this paper, the torsional response properties, both the natural periods and the center of rotation of a target RC building which has strong motion accelerometers are identified using the Subspace State Space System IDentification (4SID) with an ambient vibration record and strong motion records, where the former can reflect the current condition of the building and the latter can reflect temporal change of building conditions due to past seismic reinforcements and past experience from earthquakes. The 4SID is one of the methods which can identify parameters of a system composed of Multi-Input and Multi-Output (MIMO) in time domain. With the parameters of the method chosen correctly, it is indicated that the torsional response properties with ambient vibration records and with strong motion records agree well with each other in reasonable range. In other words, it would be possible to evaluate seismic capacity of existing eccentric RC building by ambient vibration measurement. Moreover, the long-term change of the center of rotation on the target RC building is discussed. Lastly, for the purpose of evaluating ultimate seismic capacity, the ultimate behavior of the center of rotation is investigated by an elastoplastic seismic response analysis of a single-story model with biaxially seismic eccentricity. Finally, this paper proposes evaluation procedure for ultimate seismic capacity of existing eccentric RC building by ambient vibration measurement and the system identification techniques.

Keywords: Existing seismically eccentric RC building; Ambient vibration measurement; Ultimate seismic capacity

1. Introduction

Torsional response of building is a very difficult problem. There are many researches relevant to the problems, and the background of story collapses due to torsional response has caused many researchers to work on torsional response properties. For example, the research about torsional response [1]~[4], the critical angle of ground motion [5], CQC method for plural response spectrum calculation [6], seismic reliability analysis of asymmetric buildings with normalized intensity [7], and system identification of eccentric building [8].

In this paper, for the discussions based on basic torsional response properties, applied is single-story model with biaxially seismic eccentricity. Ambient vibration, plastic seismic response and brief seismic capacity evaluation of the eccentric RC building are investigated after the verification of the system identification method. Moreover, the ultimate behavior of the torsional response properties of the model equivalent to the eccentric RC building is investigated.

2. Single-story model with biaxially seismic eccentricity

In the section 2, single-story model with biaxially seismic eccentricity is introduced. This model is used to grasp basic behavior of torsional response of a seismically eccentric building.

Figure 1 indicates single-story model with biaxially seismic eccentricity, which is assumed to have a rectangular rigid floor, as is shown in the figure. This model is seismically eccentric due to spatial non-uniformity of mass and horizontal rigidity in two orthogonal axes which are x-axis and y-axis. As regards the model, three centers; ‘G’ (the center of gravity), ‘R’ (the center of rigidity) and ‘F’ (the center of floor area) do not coincide with each other, as is shown in Figure 1.

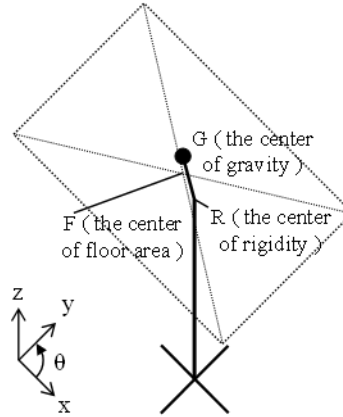


Figure 1 – Single-story model with biaxially seismic eccentricity

Figure 2 indicates the i -th eigen mode shape of the system, where i can be 1 to 3. The vector e_x and e_y are respective components of the relative distance between G and R, so called the eccentric distance respectively. X_i , Y_i and Θ_i are respective components of the i -th eigenvector. Using the vector, the i -th Center of rotation denoted by C_i is computed, and then the largest horizontal response in i -th mode on the floor denoted by D_i is found as the farthest point from the rotational center C_i . r_θ is a radius of rotation, and distribution of mass $\rho(x,y)$ and story mass m are referred to Equations (1) and (2).

$$\int_{y_{min}}^{y_{max}} \int_{x_{min}}^{x_{max}} \rho(x,y) dx dy = m \quad (1)$$

$$r_\theta = \sqrt{\frac{1}{m} \int_{y_{min}}^{y_{max}} \int_{x_{min}}^{x_{max}} \rho(x,y) (x^2 + y^2) dx dy} \quad (2)$$

Where x and y are the coordinates, and the origin is G.

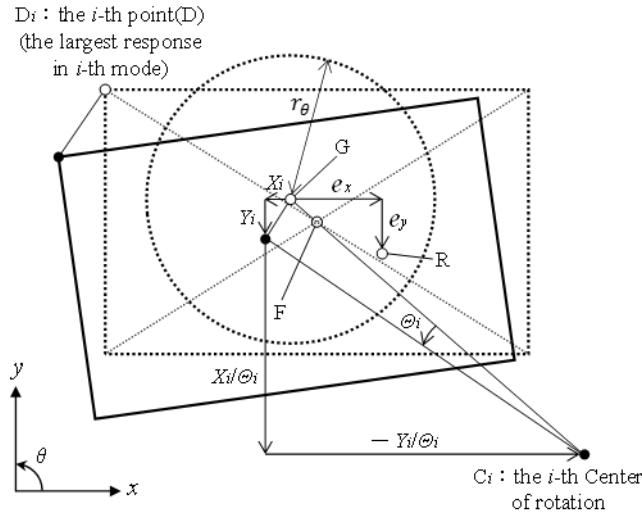


Figure 2 – i -th eigen mode shape ($i = 1\sim 3$)

Relations between the eigenvectors and the eigenvalues are derived as in the following equations.

$$-\frac{Y_i}{\theta_i} = \frac{e_x}{1 - \left(\frac{\omega_i}{\omega_y}\right)^2}, \quad \frac{X_i}{\theta_i} = \frac{e_y}{1 - \left(\frac{\omega_i}{\omega_x}\right)^2} \quad (i = 1\sim 3) \quad (3)$$

ω_i is the square root of eigenvalue, which is often called i -th natural circular frequency. ω_x and ω_y are $\sqrt{K_x/m}$ and $\sqrt{K_y/m}$ respectively, where K_x and K_y are the story rigidity in each axis.

3. Coefficient of Response Increase (CRI)

In the section 3, the new index, coefficient of response increase of the i -th mode (CRI_i), is introduced. Under the assumption of rigid body of the floor, CRI_i is defined as an increase ratio of the horizontal response at D_i to that at F , as is shown in Figure 2. CRI_i is computed in Equation (4).

$$CRI_i = \overline{C_i D_i} / \overline{C_i F} \quad (i = 1\sim 3) \quad (4)$$

CRI_i represents the torsional response index that $\overline{C_i D_i}$ (distance between C_i and D_i) is divided by $\overline{C_i F}$ (distance between C_i and F). Therefore, always, $CRI_i > 1$. If the location of C_i can be found by making ambient vibration measurement on the target building, it becomes possible to evaluate CRI_i , assuming that the location of F on the target building can be found by referring design documents.

It is very important to find accurately the center of rotation on the target building.

4. Identification of the center of rotation based on result from 4SID

In the section 4, it is described that the way of finding the center of rotation based on 4SID (Subspace State Space System IDentification) methodology [9]-[13]. In this study, the Ordinary MOESP (Multi-variable Output Error State sSpace) which is one of the 4SID algorithms will be applied to the acceleration time history data observed on the target building.

4.1 algorithm of 4SID

The method is based on the state space representation which written as following two equations [14]:



$$\mathbf{x}(t+1) = \mathbf{A}\mathbf{x}(t) + \mathbf{B}\mathbf{u}(t) \quad (5)$$

$$\mathbf{y}(t) = \mathbf{C}\mathbf{x}(t) + \mathbf{D}\mathbf{u}(t) \quad (6)$$

Where t is time, $\mathbf{x}(t)$ denotes the state vector, and $\mathbf{u}(t)$ and $\mathbf{y}(t)$ are the input and output vectors of the system, respectively. \mathbf{A} , \mathbf{B} , \mathbf{C} , and \mathbf{D} are the constant matrices.

Based on the above-mentioned equation, the following equation is obtained.

$$\mathbf{Y}_k = \mathbf{O}_r \mathbf{X}_k + \mathbf{\Psi}_r \mathbf{U}_k \quad (7)$$

Where k and r denote the step number and number of block rows, respectively. \mathbf{Y}_k , \mathbf{U}_k , \mathbf{O}_r , \mathbf{X}_k and $\mathbf{\Psi}_r$ in equation (7) are defined as follows:

$$\mathbf{Y}_k = \begin{bmatrix} \mathbf{y}(k) & \mathbf{y}(k+1) & \cdots & \mathbf{y}(k+N-1) \\ \mathbf{y}(k+1) & \mathbf{y}(k+2) & \cdots & \mathbf{y}(k+N) \\ \vdots & \vdots & \ddots & \vdots \\ \mathbf{y}(k+r-1) & \mathbf{y}(k+r) & \cdots & \mathbf{y}(k+r+N-2) \end{bmatrix} \in \mathbb{R}^{r \times N} \quad (8)$$

$$\mathbf{U}_k = \begin{bmatrix} \mathbf{u}(k) & \mathbf{u}(k+1) & \cdots & \mathbf{u}(k+N-1) \\ \mathbf{u}(k+1) & \mathbf{u}(k+2) & \cdots & \mathbf{u}(k+N) \\ \vdots & \vdots & \ddots & \vdots \\ \mathbf{u}(k+r-1) & \mathbf{u}(k+r) & \cdots & \mathbf{u}(k+r+N-2) \end{bmatrix} \in \mathbb{R}^{r \times m \times N} \quad (9)$$

$$\mathbf{O}_r = [\mathbf{C} \quad \mathbf{C}\mathbf{A} \quad \cdots \quad \mathbf{C}\mathbf{A}^{r-1}]^T \in \mathbb{R}^{r \times n} \quad (10)$$

$$\mathbf{X}_k = [\mathbf{x}(k) \quad \mathbf{x}(k+1) \quad \cdots \quad \mathbf{x}(k+r-1)] \in \mathbb{R}^{n \times N} \quad (11)$$

$$\mathbf{\Psi}_r = \begin{bmatrix} \mathbf{D}_d & \mathbf{0} & \mathbf{0} & \cdots & \mathbf{0} \\ \mathbf{C}_d \mathbf{B}_d & \mathbf{D}_d & \mathbf{0} & \cdots & \mathbf{0} \\ \mathbf{C}_d \mathbf{A}_d \mathbf{B}_d & \mathbf{C}_d \mathbf{B}_d & \mathbf{D}_d & \cdots & \mathbf{0} \\ \vdots & \vdots & \vdots & \ddots & \vdots \\ \mathbf{C}_d \mathbf{A}_d^{r-2} \mathbf{B}_d & \mathbf{C}_d \mathbf{A}_d^{r-3} \mathbf{B}_d & \mathbf{C}_d \mathbf{A}_d^{r-4} \mathbf{B}_d & \cdots & \mathbf{D}_d \end{bmatrix} \in \mathbb{R}^{r \times l \times r \times m} \quad (12)$$

Where r , l and m denote the number of block rows, output data and input data, respectively. \mathbf{O}_k written in equation (10) is called ‘‘extended observability matrix’’.

The ordinary Multi-variable Output Error State sSpace (MOESP), the one of the system identification method, was used in this paper. This method is performed based on the following equation.

$$\mathbf{G}_k = \mathbf{Y}_k / \mathbf{U}_k^\perp = \mathbf{Y}_k \mathbf{\Pi}_{\mathbf{U}_k}^\perp \quad (13)$$

Where, $\mathbf{Y}_k / \mathbf{U}_k^\perp$ is formed by projecting the row space of \mathbf{Y}_k on the orthogonal complement of the row space of \mathbf{U}_k . $\mathbf{\Pi}_{\mathbf{U}_k}^\perp$ is the geometric operator that projects the row space of a matrix onto the orthogonal complement of the row space of the matrix \mathbf{U}_k . From equations (7) and (13), we obtain

$$\mathbf{G}_k = \mathbf{O}_r \mathbf{X}_k \mathbf{U}_k^\perp \quad (14)$$

Then, a singular value decomposition of matrix \mathbf{G}_k is performed following equation.

$$\mathbf{G}_k = \mathbf{U}\mathbf{S}\mathbf{V}^T \approx \mathbf{U}_1 \mathbf{S}_1 \mathbf{V}_1^T \quad (15)$$

Where \mathbf{U} and \mathbf{V} are orthogonal matrices, the left and right singular matrix, respectively. \mathbf{S} is the diagonal matrix of singular values of \mathbf{G}_k , while \mathbf{S}_1 , \mathbf{U}_1 , and \mathbf{V}_1 are, respectively, the diagonal matrix of the singular values, and the

left and right singular matrix when excluding the extremely small singular values. The system order can be estimated from the size of matrix \mathbf{S}_1 .

Then, the extended observability matrix \mathbf{O}_k can be identified by the following equation.

$$\mathbf{O}_k = \mathbf{U}_1 \mathbf{S}_1^{1/2} \quad (16)$$

Then, the matrix \mathbf{A} can be identified as follow.

$$\mathbf{A} = \underline{\mathbf{O}_k}^\dagger \overline{\mathbf{O}_k} = \begin{bmatrix} \mathbf{C} \\ \mathbf{CA} \\ \vdots \\ \mathbf{CA}^{r-2} \end{bmatrix}^\dagger \begin{bmatrix} \mathbf{CA} \\ \mathbf{CA} \\ \vdots \\ \mathbf{CA}^{r-1} \end{bmatrix} \quad (17)$$

The natural frequency of j -th mode, f_j , was calculated by using:

$$f_j = \frac{|\ln \lambda_j|}{2\pi\Delta t} \quad (18)$$

Where λ_j is the j -th eigenvalue of the matrix \mathbf{A} in a discrete time system and Δt the sampling period. Furthermore, the j -th eigen mode shape vector Φ_j is calculated as follow.

$$\Phi_j = \mathbf{C}\varphi_j \quad (19)$$

φ_j is the j -th eigen vector of matrix \mathbf{A} .

4.2 Accuracy of 4SID

The process of verification by elastic seismic response analysis is as follows:

i) Model for verification

In order to verify the system identification technique, Figure 3 shows the target model, which is a single-story model with biaxially seismic eccentricity. The floor is assumed to behave as a rigid body.

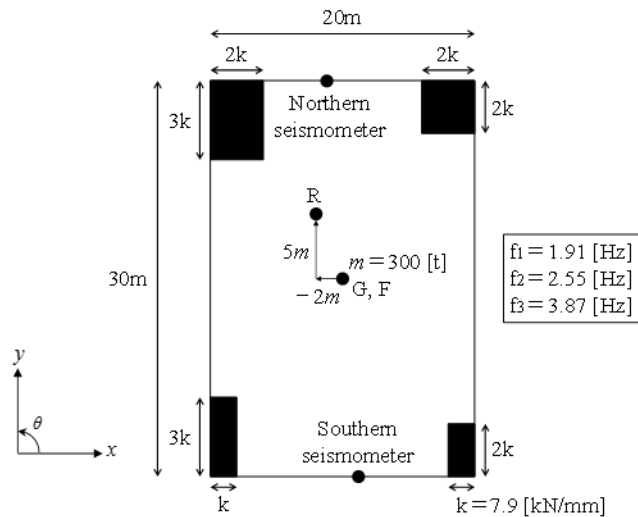


Figure 3 – Target model



ii) Input

Table 1 indicates list of inputs which are seismic waves. The duration of each wave is as follows: ELC is 53.46[s], HAC is 50.98[s], TAF is 54.36[s], TOH is 40.94[s].

Table 1 – List of inputs (seismic waves)

Abbreviation (duration)	Name of seismic wave	Observation point (direction)	Input direction
ELC_EW (53.46[s])	Imperial valley earthquake (1940)	El Centro (EW)	x
ELC_NS (53.46[s])	Imperial valley earthquake (1940)	El Centro (NS)	y
HAC_EW (50.98[s])	Tokachi trench earthquake (1968)	Hachinohe harbor (EW)	x
HAC_NS (50.98[s])	Tokachi trench earthquake (1968)	Hachinohe harbor (NS)	y
TAF_EW (54.36[s])	California earthquake (1952)	Kern country (EW)	x
TAF_NS (54.36[s])	California earthquake (1952)	Kern country (NS)	y
TOH_EW (40.94[s])	Miyagi trench earthquake (1978)	The University of Tohoku (EW)	x
TOH_NS (40.94[s])	Miyagi trench earthquake (1978)	The University of Tohoku (NS)	y

iii) Parameters of analysis

Parameters of analysis are as follows. Time integration method is Newmark – β ($\beta = 0.25$). Integration time is 0.02[s]. Damping ratio is 3[%] in all of 3 modes. Input point is under ‘G’ and is on the first floor. Output points are ‘Northern seismometer’ and ‘Southern seismometer’. Therefore, the 2-inputs-and-4-outputs system is identified using 4SID as single-story model with biaxially seismic eccentricity.

iv) Parameters of 4SID

Segmented time length of time history data (input waves and output waves) for running system identification is 20[s], as is denoted by T in Figure 4. Intervals of running are 10[s]. Sampling frequency is 50[Hz]. Model order is 6 (for finding 3 modes). The number of block rows is 20.

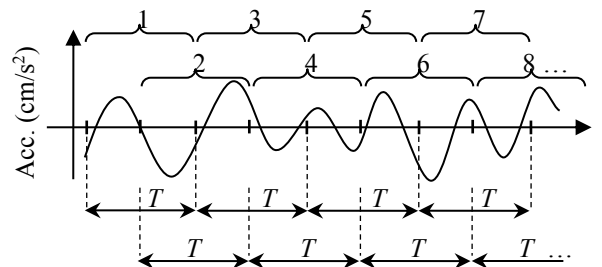


Figure 4 – Segmented time length of time history data for running system identification

Figure 5 indicates the way of finding the center of rotation based on the eigenvectors which are identified at the each output point.

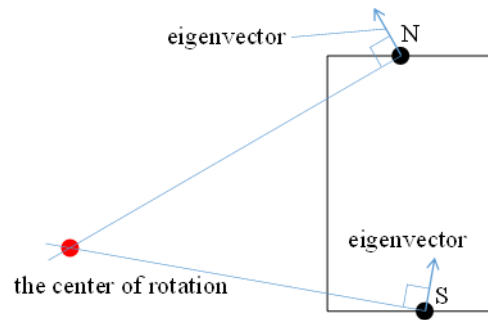


Figure 5 – Way of finding the center of rotation based on identified eigenvectors

Figure 6 indicates the center of rotation using 4SID with all waves (all inputs and outputs) and by eigenvalue analysis. It is confirmed that the 4SID can give good results that all the centers of rotation in all the modes from 4SID agree with the fundamental behavior of the model.

Figure 7 indicates the center of rotation reflecting observation noise. The noise is white noise which conforms normal distribution (the mean is 0[mm/s²], and standard deviation is 1[mm/s²]). Signal-noise ratio are 48 ~ 55[dB] in all the inputs of Table 1. It is inferred that in case the each direction of the eigenvectors which are identified with noise is nearly parallel to each other, the target center of rotation becomes uneven. The identification error by noise causes more variability of the center of rotation in that case.

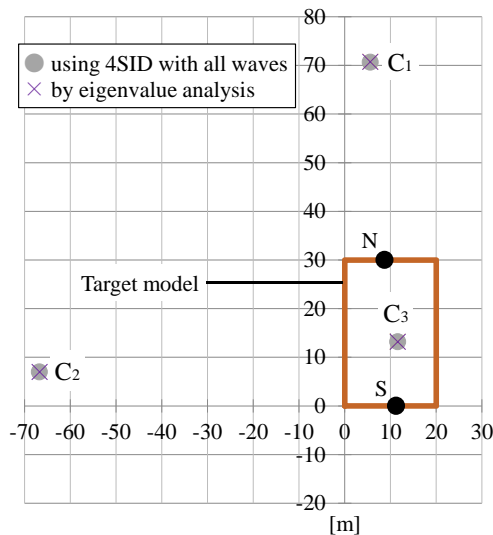


Figure 6 – The center of rotation using 4SID

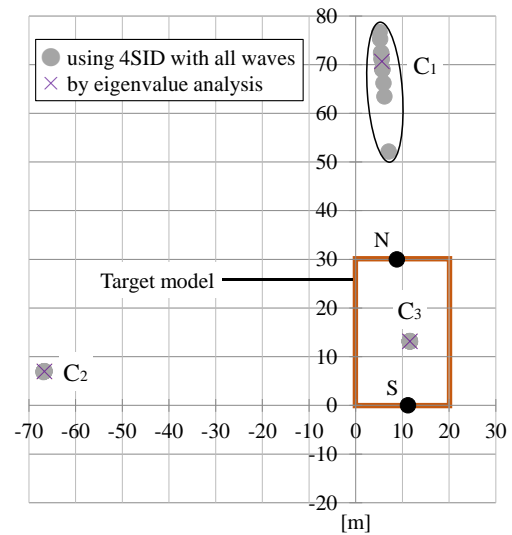


Figure 7 – The center of rotation using 4SID with noise

5. C_i of the target building

In the section 5, evaluation seismic capacity by ambient vibration measurement and long-term change of the C_i of the target building are investigated.

5.1 Target building

The target RC building is 11th building of the department of engineering in Hongo campus. The building was completed in 1968, and had reinforcement works in 2006. The building has 9 stories above the ground level and 2 stories below the ground level, moreover which has L-shaped plan as is seen in Figure 8. Figure 8 indicates appearance of the target building and plan of 7th story above the ground. The system of the target building is identified to single story (the stories from 1st to 7th above the ground are identified to single story) model with

biaxially seismic eccentricity, using 4SID with an ambient vibration record and strong motion records which are recorded at 3 micrometers and 5 seismometers respectively. 1 micrometer and 1 seismometer are set on the floor of 1st story.

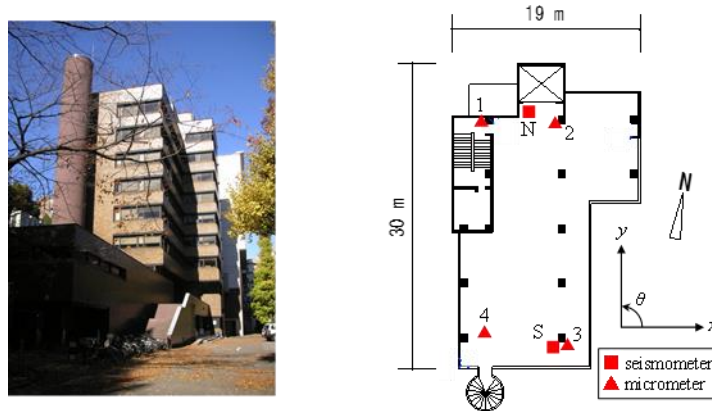


Figure 8 – Appearance of the target building (left) and Plan of 7th story above ground (right)

Table 2 indicates outline of the strong motion records and ambient vibration record on the target building, which shows abbreviation (name for groups of recorded waves), date of recording in Japan time, the number of records in each group and PGA (Peak Ground Acceleration) in each direction. Sampling frequency of the strong motion records and ambient vibration record are 100[Hz] and 200[Hz] respectively. After sampling, all the waves go through 1~5[Hz]-band-pass filter and are sampled down to 20[Hz]. The parameters of 4SID are the same as 4.2.iv) except sampling frequency, though there is difference in the number of outputs between the strong motion records and ambient vibration record.

Table 2 – Outline of the strong motion records and ambient vibration record on the target building

Abbreviation	Date (Japan time)	The number of records	PGA[Gal] (x-direction, y-direction)
before 3.11	2007.1.9 ~ 2009.8.11	46	1.5 ~ 45.9 , 1.4 ~ 36.4
3.11 main shock	2011.3.11	1	218.1 , 197.0
after 3.11	2011.3.11 ~ 2014.9.16	11	7.4 ~ 91.0 , 6.5 ~ 64.1
AVM after 3.11	2015.2.24 (15:18 ~ 15:38)	1	1.4 , 1.4

5.2 C_i by ambient vibration measurement and strong motion records

C_i and natural periods by ambient vibration measurement are indicated in Figure 9. In 1st mode response, the stimulus in x -direction is dominant. In 2nd mode response, the stimulus in y -direction is dominant. In 3rd mode response, the stimulus in θ -direction is dominant. Therefore, the response which is reflecting all the modes depends on the components of input wave in each direction.

It is very interesting to see the results from the analysis on C_i and natural periods from strong motion records, which are plotted in Figure 10. In 1st mode response, the component of eigenvector in θ -direction had been increased after 3.11 main shock. As regards C_i , the other two modes had not been changed after 3.11 main shock. However, as regards natural periods, they had been increased by 10 percent after 3.11 main shock in all the modes. It is inferred that some damage in parts from 3.11 main shock causes the change. Moreover, it is inferred that there is more damage on southern parts in x -direction.

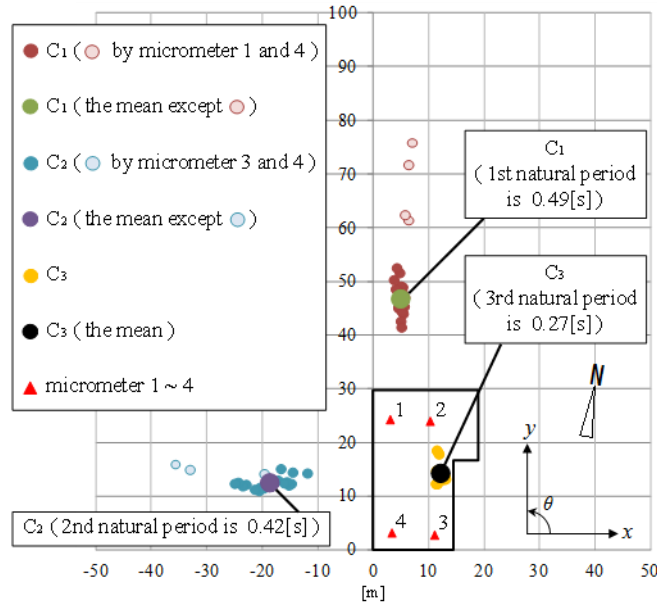


Figure 9 – C_i by ambient vibration measurement

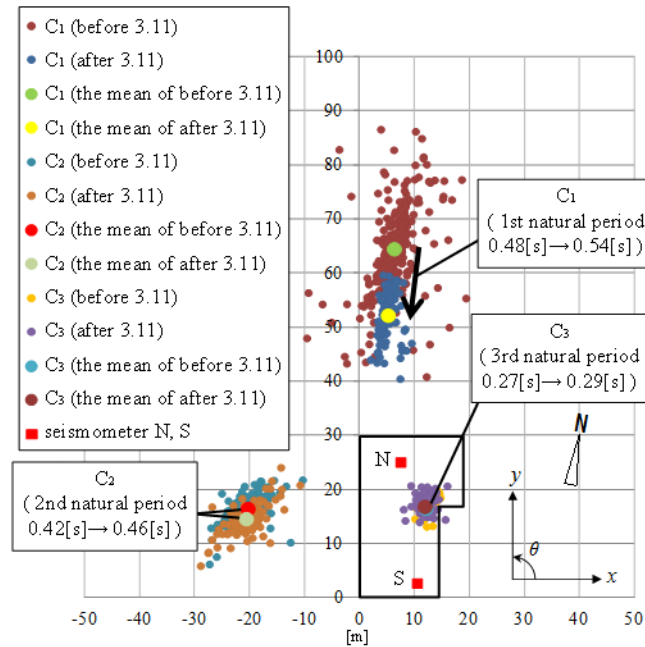


Figure 10 – C_i by strong motion records

In comparison of Figure 9 and Figure 10, C_i by ambient vibration measurement and strong motion records after 3.11 agree well with each other. The natural periods by ambient vibration measurement are shorter than by strong motion records after 3.11 by 10 percent in all the modes. It is inferred that more amplitude of vibration causes natural period to be longer. The degree of the change can depend on the scale of target building and amplitude of building vibration.

5.3 Brief evaluation of seismic capacity with CRI_i and natural periods by ambient vibration measurement

Table 3 indicates CRI_i and D_i by ambient vibration and strong motion on the target building, which shows target C_i (the mean) on Figure 9 or Figure 10 (which group of recorded waves is used), CRI_i and coordinates of D_i on Figure 9 or Figure 10. In 1st and 2nd mode response where the stimulus in x -direction and in y -direction are dominant respectively, CRI_i and D_i by ambient vibration and strong motion after 3.11 agree well with each other.

Table 3 – CRI_i and D_i by ambient vibration and strong motion on the target building

C_i by what	$CRI_1, D_1(\text{coordinates})$	$CRI_2, D_2(\text{coordinates})$	$CRI_3, D_3(\text{coordinates})$
ambient vibration	1.54, (13.9, 0)	1.52, (18.6, 29.9)	4.65, (0, 29.9)
strong motion after 3.11	1.46, (13.9, 0)	1.46, (18.6, 29.9)	5.48, (0, 0)
strong motion before 3.11	1.34, (13.9, 0)	1.44, (18.6, 29.9)	5.27, (0, 0)

Figure 11 indicates maximum story drift (by translation input in a single direction) of the target building model (with the displacement response spectrum for seismic design). Maximum story drift is not in which story but at which point in a story. In other words, maximum story drift is the displacement response at D_i . Figure 11 shows the two maximum story drift by translation input in a single direction (x and y respectively). The maximum story drift is calculated, multiplying CRI_i by the displacement based on response spectrum for seismic design. As regards the seismic design standard in this paper, maximum acceleration of input is 490[Gal]. CRI_i and natural periods by ambient vibration measurement is applied to the calculation.

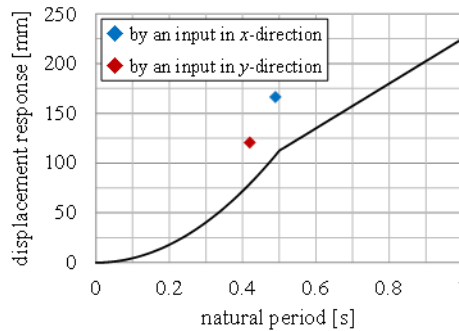


Figure 11 – Maximum story drift of the target building model

Table 4 – Maximum story drift angle of the target building model

Direction of input	Maximum story drift angle (reference point)
x	1/131 (the edge in southeast)
y	1/180 (the edge in northeast)

Table 4 indicates maximum story drift angle of the target building model, which can be referred to by current seismic design standards in Japan.

6. Behavior of C_1 to the ultimate

In the section 6, it is investigated about behavior of C_1 to the ultimate. The model in 4.2.i) is applied to the target model in this section. Restoring force characteristics (Degrading tri-linear model [15]) are shown in Figure 12, where k_0 is the initial rigidity of each column (in Figure 3). The input is 16.5 times of 3.11 main shock in Table 2, which is shown in Figure 13. The input direction is only x . There is no noise on the input nor the outputs.

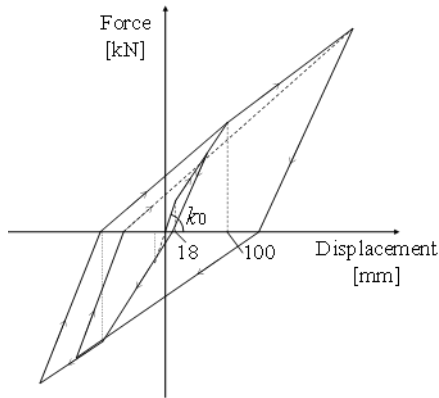


Figure 12 – Restoring force characteristics

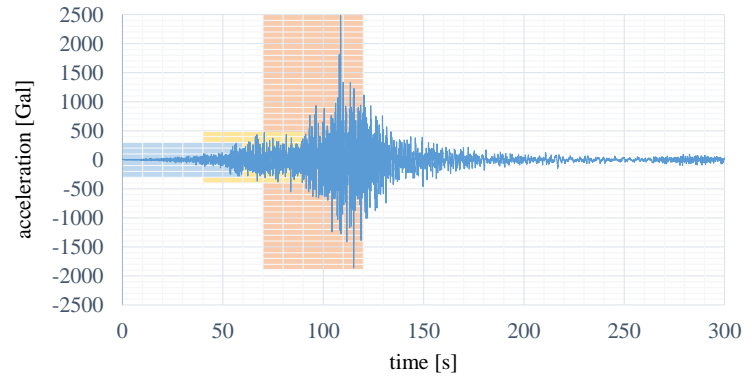


Figure 13 – Input seismic wave (16.5 times of 3.11 main shock)

Figure 14 indicates behavior of y -coordinates of C_1 during the seismicity (16.5 times of 3.11 main shock). Until 50[s] (60[s] in Fig. 13), or while the degree of amplitude is about the same as the original 3.11 main shock, C_1 approached the model and it is confirmed that the distance between C_1 at 10[s] (equal to by eigenvalue analysis) and at 50[s] of the model is the same as the distance between C_1 before and after 3.11 main shock of the target building. As regards the behavior, the southern columns of the model exceeded the first-plastic displacement. Until 80[s] from 50[s] (40 ~ 90[s] in Fig. 13), C_1 got away the model. As regards the behavior, the northern columns also exceeded the first-plastic displacement. In other words, just the balance of distribution of horizontal rigidity is improved. Until 110[s] from 80[s] (70 ~ 120[s] in Fig. 13), C_1 approached the model again. The southern columns exceeded the second-plastic displacement.

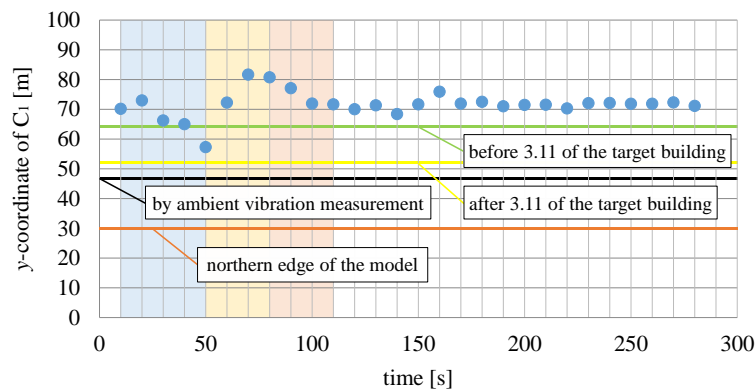


Figure 14 – Behavior of y -coordinates of C_1 during the seismicity (16.5 times of 3.11 main shock)

7. Conclusion

The state of the target RC building after 3.11 main shock agreed with the state that C_1 of the equivalent model got to most near point from northern edge of the model (at 50[s] in Fig. 14). For brief evaluation of ultimate seismic capacity of existing seismically eccentric RC building by ambient vibration measurement, required are the further investigations about the relation between restoring force characteristics and ultimate behavior of C_i . The results and conclusions in this paper are as follows.



- 1) CRI_i is defined in the section 3 as torsional response index, which is applied to brief evaluation of seismic capacity by ambient vibration measurement in the section 5.3.
- 2) It is verified that the way of finding C_i using 4SID (Subspace State Space System IDentification) is proper in the section 4. Moreover, it is investigated that improper arrangement of seismometer (or micrometer) make it difficult finding the exact location of C_i with observation noise.
- 3) With the parameters of 4SID chosen correctly, it is indicated that the C_i by ambient vibration measurement and by strong motion records agree well with each other in the section 5. Moreover, the seismic capacity of the target building is evaluated briefly with C_i and natural periods by ambient vibration measurement.
- 4) As regards the long-term change of C_i on the target building, only C_1 approached the building after 3.11 main shock in 2011.
- 5) Behavior of C_1 on the target model to the ultimate is investigated in the section 6. The investigation indicates that C_i does not just approach the target building, and indicates that there is the case that C_i approaches and gets away target building over and over to the ultimate.

8. Acknowledgements

The authors thank Dr. Kashima of the Building Research Institution in Japan for providing us with the strong motion records.

9. References

- [1] Yutaka Yamazaki (1986): Lateral torsional response of buildings during earthquakes. *Journal of Structural and Construction Engineering*, **369**, 31-41.
- [2] Jun Sakamoto, Yoshiro Kohama, Masao Watanabe, Takashi Tuji (1987): Torsionally coupled response of shear-type buildings to earthquake ground motion. *Journal of Structural and Construction Engineering*, **380**, 22-31.
- [3] Koichi Ohami, Masaya Murakami (1999): Indices of effects of torsional coupling on earthquake response of 1-story linear systems with uniaxial eccentricity. *Journal of Structural and Construction Engineering*, **521**, 25-32.
- [4] Kenji Fujii (2013): Torsional index of single-story asymmetric building model for application of seismic response evaluation using equivalent sdof model. *Journal of Structural and Construction Engineering*, **684**, 299-308.
- [5] Oscar A Lopez, Ronald Torres (1997): The critical angle of seismic incidence and the maximum structural response. *Earthquake Engineering & Structural Dynamics*, **26**, 881-894.
- [6] EL Wilson, A Der Kiureghian, EP Bayo (1981): Short communications, a replacement for the SRSS method in seismic analysis. *Earthquake Engineering & Structural Dynamics*, **9**, 187-194.
- [7] Yasser Picazo, Orlando Diaz Lopez, Luis Esteva (2014): Seismic reliability analysis of buildings with torsional eccentricities. *Earthquake Engineering & Structural Dynamics*, Wiley Online Library, 10.1002/eqe.2509.
- [8] Chin-Hsiung Loh, Jian-Huang Weng, Chia-Hui Chen, Kung-Chun Lu (2013): System identification of mid-story isolation building using both ambient and earthquake response data. *Structural Control & Health Monitoring*, **20**, 139-155.
- [9] M. Verhaegen and P. Dewilde (1992): Subspace model identification, Part 1: The output-error state-space model identification class of algorithms, *International Journal of Control*, **56** (5), 1187-1210.
- [10] M. Verhaegen (1994): Identification of the deterministic part of MIMO state space models given in innovations form from input-output data, *Automatica*, **30** (1), 61-74.
- [11] L. Ljung (1999): *System Identification – Theory for the user – second edition*, Prentice Hall.
- [12] P. Van Overschee and B. De Moor (1996): *Subspace Identification for Linear Systems*, Kluwer Academic Pub.
- [13] T. Katayama (2005): *Subspace Methods for System Identification*, Springer.
- [14] T. Kailath (1980): *Linear Systems*, Prentice-Hall, Englewood Cliffs, New Jersey.
- [15] T. Takeda, M. A. Sozen and N. Norby (1970): Reinforced Concrete Response to Simulated Earthquakes, *Journal of the Structural Division, Proceedings of the ASCE*, **96**(ST12), 2557-2573.